引用格式：ZHU Dongxu, GONG Yuting, LIU Wei, et al. Differential Two-wave Mixing Interferometer for Micro-vibration Detection[J]. Acta Photonica Sinica, 2023, 52(6):0612002
朱东旭,龚玉婷,刘维,等.差动式双波混合干涉微小振动检测系统[J].光子学报,2023,52(6):0612002

差动式双波混合干涉微小振动检测系统

朱东旭[1],龚玉婷[1],刘维[1],孔明[1],王道档[2]
(1 中国计量大学 计量测试工程学院,杭州 310018)
(2 亚利桑那大学 光学科学学院,美国 图森 85721)

摘　要:针对工业环境下粗糙金属表面微小振动的在线测量需求,提出了一种基于差动式双波混合干涉的微小振动检测系统。该系统将极性相反的高电压分别施加在两块硅酸铋晶体上以得到差动式双路振动解调信号,进而通过差分处理抑制对电压极性不敏感的噪声并提高灵敏度。为验证所提出方案的可行性,分别进行了仿真分析与实验验证。对一粘连在压电陶瓷上的紫铜片进行振动测量实验,并将振动测量结果分别与施加在压电陶瓷上的电压和激光测振仪的测量结果进行对比。结果表明,利用所提出检测系统可准确获得振动信号的频率、相位和幅值信息,与单路式结构相比,差动式双波混合干涉仪的灵敏度提高了一倍,信噪比从27.47 dB提高到了30.83 dB,相对误差的均方根值从3.07%降低到了1.42%。

关键词:双波混合干涉;差动式;微小振动检测;噪声抑制;硅酸铋晶体
中图分类号:TH741　　**文献标识码**:A　　**doi**:10.3788/gzxb20235206.0612002

0　引言

随着现代制造和检测技术的飞速发展及广泛应用,金属粗糙表面微小振动检测技术在众多领域发挥着重要作用[1-4],包括材料分析、无损检测和机械系统动态分析等。目前的振动检测主要分为接触式和非接触式。压电换能器作为一种通用性较强的高精度接触式测量工具,被广泛应用于振动检测[5-6]。但其带宽有限,且通常需要通过使用耦合剂紧贴在在被测试件表面,故无法对高温、腐蚀性或高曲率表面进行检测,接触法由于工作距离和耦合剂的限制,难以真正满足完全非接触式的在线测量应用要求。与传统的接触式振动检测技术相比,光学法是完全非接触检测方法。光学法可分为干涉法和非干涉法(包括激光三角法和光散斑法等),非干涉法[7-8]原理简单,成本低廉,但该技术一般受制于光强接收装置的灵敏度,故测量精度、分辨力十分有限。学者们对零差、外差和激光多普勒等干涉检测技术展开研究,并开发了相应的应用装置[9-12],但此类干涉检测技术无法消除环境引起的缓慢相位漂移[13-14],且存在测量粗糙表面时所引起的波前不匹配等问题,故通常只适用于实验室条件下光滑表面的振动探测。针对工业环境下粗糙表面振动检测的需求,一种新型的双波混合干涉测量系统[15-16]被学者们提出,在双波混合干涉的过程中,光折变晶体相当于一个自适应的分束器,失真的信号光和参考光在光折变晶体中得到实时修正再进行干涉,进而能够自动减小由相位波动引起的低频噪声(如空气扰动、热变形等)[17]。但传统的双波混合干涉仪不能抑制光强波动或电噪声的干扰[18],故系统的稳定性与信噪比受到了限制,且系统的灵敏度易受到光电探测器的饱和光功率的抑制。

为了提高传统的双波混合干涉仪的灵敏度和抗噪声能力,本文提出了一种差动式双波混合干涉微小振动检测系统。系统选用双光路设计并在双路光折变晶体上施加极性相反的高电压以获得差动式双路信号,

基金项目:浙江省自然科学基金(No. LY21E050016),国家自然科学基金(No. 51775528)
第一作者:朱东旭,1210949335@qq.com
通讯作者:刘维,liuw@cjlu.edu.cn
收稿日期:2022-12-12;**录用日期**:2023-01-03

向双路信号采用差分处理进而抑制对电压极性不敏感的噪声和单次测量误差，并提高系统的灵敏度。针对工业环境下粗糙表面微小振动的高灵敏度检测需求，对所涉及系统关键元件的选择、布局设计以及物理模型进行研究分析。

1 原理

1.1 基于差动式双波混合干涉的测量系统布局

用于振动检测的差动式双波混合干涉仪的系统光路布局如图1所示。单纵模激光器(Laser)发出532 nm波长的激光光束，经过扩束器(Beam Expander，BE)、偏振片(Polarizer，P)、二分之一波片(Half Wave Plate，HWP)后得到直径4 mm的线偏振光，随后入射至偏振分光棱镜(Polarized Beam Splitter 1，PBS1)分成两路相干光：其中s分量反射光作为参考光，经折光反射镜(Mirror，M2)后被分光棱镜(Beam Splitter 1，BS1)分成两部分，其中透射光和反射光被折光反射镜(M3、M5)反射后分别进入硅酸铋(BSO，$Bi_{12}SiO_{20}$)光折变晶体(BSO1、BSO2)；p分量透射光为信号光，通过偏振分光棱镜(PBS2)后经过1/4波片(Quarter Wave Plate，QWP)变为圆偏振光，经望远系统(Galileo Telescopic System，GT)后被物镜(Lens，L1)会聚至紫铜片(粗糙度的轮廓算术平均偏差Ra值为6.3 μm)，紫铜片被粘连在压电陶瓷(Piezoelectric Transducer，PZT)上并被信号发生器(Signal Generator，SG)输出正弦信号驱动做正弦振动，信号光被振动信号调制后由物镜(L1)收集并沿原路返回，再次通过望远系统(GT)与1/4波片(QWP)并被转换为s线偏振光，随后经偏振分光棱镜(PBS2)反射后到达分光棱镜(BS2)，其透射光和反射光分别进入光折变晶体(BSO1、BSO2)。光折变晶体(BSO1、BSO2)中的信号光和参考光汇合叠加产生干涉。由于光折变效应，干涉条纹对晶体的折射率进行调制形成动态全息光栅并发生双波混合效应，从而产生信号光与参考光之间的能量耦合。在两块光折变晶体(BSO1、BSO2)上施加极性相反的高电压，导致两光路能量耦合的方向相反进而得到双路差动信号。出射晶体的两路光强信号分别被光电二极管(photodiode，pd1、pd2)探测，利用计算机(PC)控制数据采集卡(Data Acquisition Card，DAC)对光电二极管输出的电压信号进行实时采集与处理，从而得到紫铜片的振动信号。

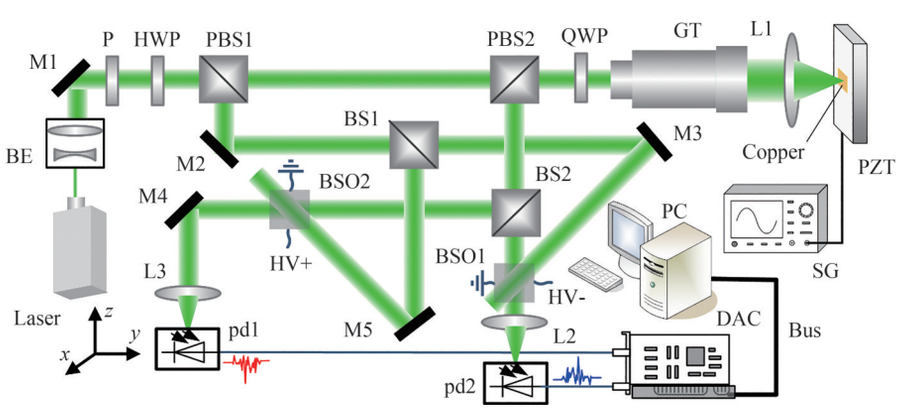

图1 差动式双波混合干涉仪系统布局

Fig.1 System layout of differential two-wave mixing interferometer

1.2 物理模型

光折变晶体的光折变效应是差动式双波混合干涉的重要物理基础。所谓光折变效应是指在光场辐照的作用下，电光材料的折射率随着光强的空间分布变化而产生变化，从而形成动态全息光栅。如图2所示，从被测工件表面反射的信号光束与参考光束在光折变晶体中干涉从而形成动态全息光栅，参考光束通过该动态光栅，使其在动态全息光栅中衍射进而形成一个与信号光波前相同的“畸变”参考光束，它与携带了振动信息而“畸变”的信号光束再相干涉，进而将信号光的微小相位调制解调至出射晶体的光强中，通过光电二极管检测干涉后的光强信号从而得到被测振动信号。

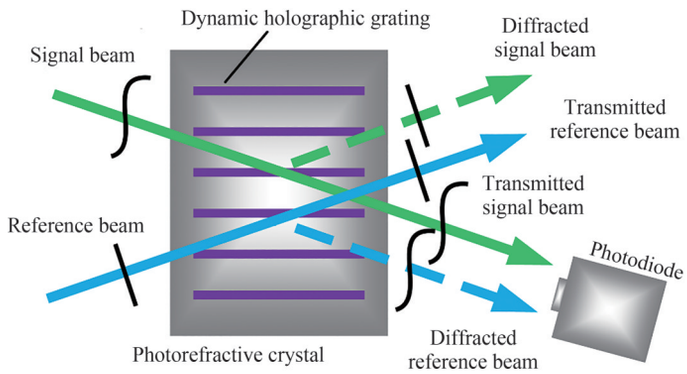

图2　光折变晶体双波混合原理

Fig.2　Schematic diagram of two-wave mixing interference in photorefractive crystal

参考光与信号光在光折变晶体内干涉后的光强分布可表示为

$$I=I_0+E_sE_r^*\exp(-\mathrm{i}\boldsymbol{K}\cdot\boldsymbol{r})+E_s^*E_r\exp(\mathrm{i}\boldsymbol{K}\cdot\boldsymbol{r}) \tag{1}$$

式中，I_0为激光器光强，E_s和E_r分别为信号光和参考光振幅，$\boldsymbol{K}=\boldsymbol{k}_s-\boldsymbol{k}_r$，$\boldsymbol{k}_s$和$\boldsymbol{k}_r$分别为信号光与参考光波矢，$\boldsymbol{r}$为矢径。

被干涉光强调制的硅酸铋光折变晶体的折射率可表示为

$$n=n_0+\frac{n_1E_sE_r^*}{2I_0}\exp\left[-\mathrm{i}(\varphi+\boldsymbol{K}\cdot\boldsymbol{r})\right]+\frac{n_1E_s^*E_r}{2I_0}\exp\left[\mathrm{i}(\varphi+\boldsymbol{K}\cdot\boldsymbol{r})\right] \tag{2}$$

式中，n_0为无光场辐照下晶体的折射率，$n_1=n_0^3\gamma E$，γ为有效电光系数，E是总电场，φ为晶体折射率分布与干涉光强分布的相位差并可被表示为

$$\varphi=\arctan\frac{E_0^2+E_d^2+E_dE_s}{E_0E_s} \tag{3}$$

式中，E_0为外电场，E_d为扩散场，E_s为饱和场。

被调制在信号光相位中的振动信号可由出射晶体的光强I_{output}得到，即

$$I_{output}=\frac{I_0}{1+m\exp(\Gamma z)}\exp(-\alpha z) \tag{4}$$

式中，m为参考光与信号光的光强比，光强耦合系数$\Gamma=2\pi n_1\sin\varphi/\lambda$，$\lambda$为光波长，$z$为晶体厚度，$\alpha$为晶体的吸收系数。

由式(4)得，光强耦合系数Γ的极性决定了信号光和参考光的光强耦合方向，在两块BSO晶体上施加相反极性的高电压使得两路差动信号的光强耦合方向相反。如图3所示，正极性高电压使晶体折射率分布与干涉光强分布的相位差φ接近0，于是输出光强I_{output}的极性与振动信号的极性相反，而负极性的高电压得到与振动信号极性相同的输出信号，晶体两端施加的电压越高，相位差φ便越接近0或π，系统对振动信号的响应便越敏感。

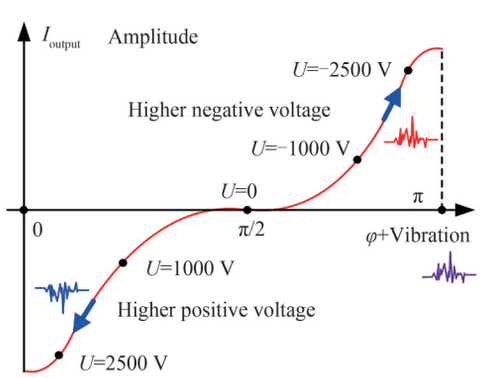

图3　差动双路信号原理

Fig.3　Schematic diagram of differential dual-path signal

2 仿真分析

为验证所提出差动式双波混合干涉仪的可行性与噪声抑制能力，基于差动式双波混合干涉仪的物理模型对其进行仿真分析，仿真中涉及的BSO晶体的参数如表1所示。

表1 光折变晶体BSO的物理参数

Table 1 Physical parameters of photorefractive crystal BSO

Parameter	Value
Thickness	5 mm
Refractive index	2.53
Electro-optic coefficient	5×10^{-10} cm/V
Absorption coefficient	2.3 cm^{-1}
Dark conductivity	$1.6\times10^{-15}\ \Omega^{-1}cm^{-1}$
Photo conductivity	$1.6\times10^{-15}\ \Omega^{-1}cm^{-1}+7.3\times10^{-8}\ I_1\Omega^{-1}cm^{-1}$

2.1 可行性验证

由式(2)可得，晶体折射率由于受到干涉条纹的调制而呈现正弦分布，但其相位与干涉条纹不一致，两者的相位差φ决定了式(4)的偏置点位置从而影响输出信号的极性，根据式(3)相位差φ的计算公式可知，施加的外电场E_0会直接影响相位差φ。当晶体的外电场E_0远大于扩散场E_d但小于饱和场E_s时，晶体两端电压对相位差的影响如图4所示，负极性的高电压使得相位差φ接近π，而正极性的高电压确保相位差φ靠近0，对晶体施加的电压越高，其相位差便越接近0或π。

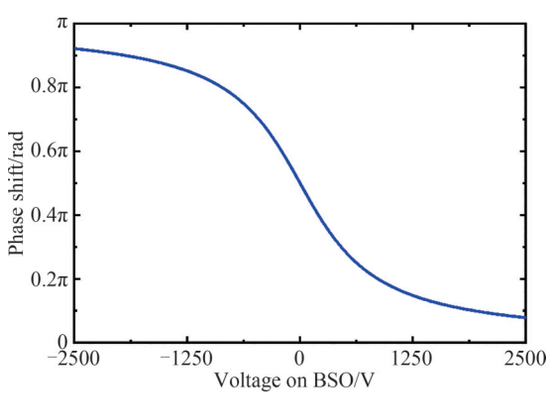

图4 仿真中晶体两端电压对相位差的影响

Fig.4 Influence of voltage applied to BSO crystal on phase shift in simulation

当被测试件做正弦振动，其频率为2 000 Hz，幅值为10 nm，由式(4)可得差动式双波混合干涉仪输出的双路信号，其中参考光与信号光的光强比m设置为1，激光器的光功率设置为207.7 mW，参考光与信号光的夹角为9°。如图5所示，双路输出信号均可准确获得被测信号的频率与波形信息，正极性的高电压使得相位差φ接近0，从而使得输出信号对振动信号的灵敏度为负，故输出信号的极性与振动信号极性相反，而负极性高电压导致了正相关的灵敏度，由此可得差动式双路输出的电压信号。

将双路输出电压信号做差分处理可得差动式双波混合干涉仪的差分输出，为分析振动幅值对差分输出信号的影响，将不同幅值的正弦振动信号带入式(4)并计算输出信号的幅值，所得结果如图6所示，在振动幅值范围0 nm至40 nm，差分输出电压与振动幅值成近似线性关系，随着振动幅值的增大，输出信号幅值与振动幅值成正相关。因此，在两块BSO晶体上施加不同极性的高电压可获得差动式双路输出，由此得到的差分输出信号可准确描述被测振动信号的波形、幅值和频率信息。

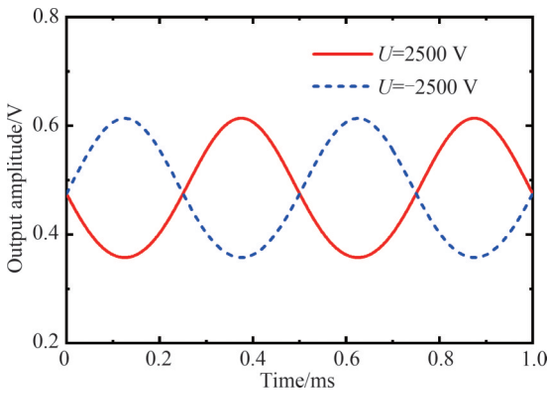

图5　仿真中差动式双路输出信号时域图

Fig.5　Time domain diagram of dual-path differential output signal in simulation

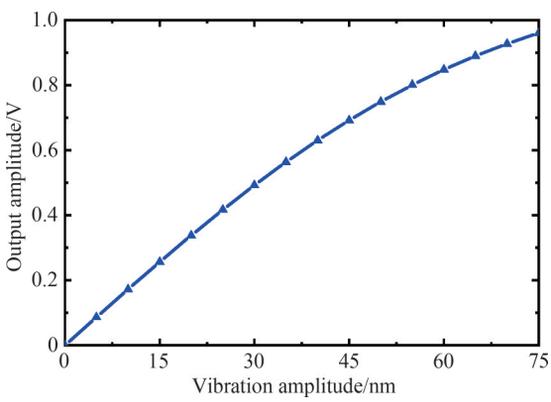

图6　仿真中差分输出信号与振动幅值的关系

Fig.6　Relationship between differential output signal and measured vibration amplitude

2.2　噪声抑制能力分析

为验证所述系统的噪声抑制能力，基于图5的仿真结果，在激光器光强I_0上添加均方根（Root Mean Square，RMS）值为0.4 mW/mm²、均值为0 mW/mm²的高斯噪声及幅值为0.2 mW/mm²、频率为4 kHz的正弦噪声，其振动检测结果如图7(a)所示，单路输出的电压信号明显受到添加噪声的影响，其信噪比为13.32 dB，经过差分处理，噪声得到抑制，所述系统的信噪比提高到了28.26 dB并且灵敏度提高了一倍。单路和差分输出的电压信号频谱分析如图7(b)所示，二者的主频均为振动信号的频率（2 kHz），与单路输出相比，差分输出频谱图中4 kHz处的正弦噪声及其6 kHz处的谐波噪声均得到抑制，且高斯噪声的幅值明显得到降低。因此，差动式双波混合干涉仪的抗噪声干扰能力明显优于传统的单路式双波混合干涉仪。

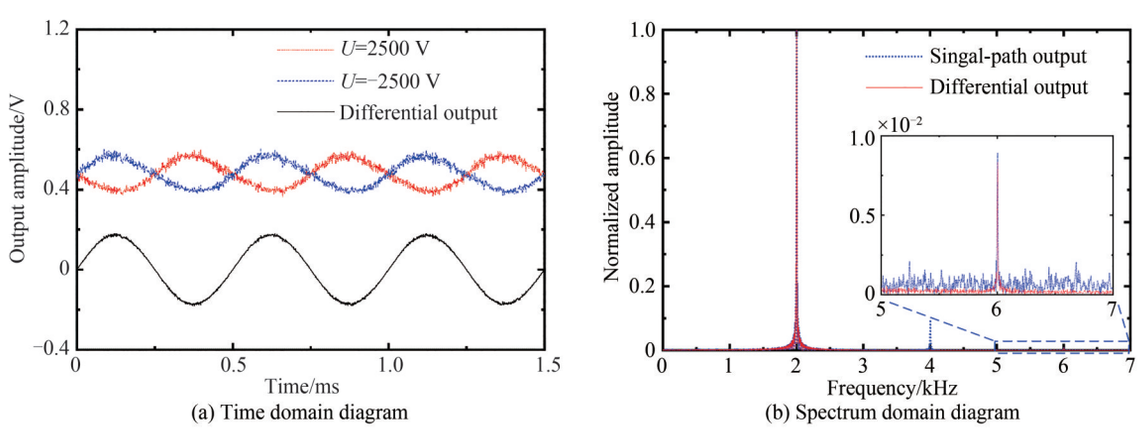

图7　仿真中添加噪声时的振动检测结果

Fig.7　Measurement result of vibration with noise in simulation

3 实验及结果分析

为了进一步验证所提出用于微小振动检测的差动式双波混合干涉仪的可行性，根据图1搭建了测量实验系统，对做正弦振动的紫铜片（粘连在压电陶瓷PZT上）进行测量，并将测量结果分别与施加在PZT的电压和激光测振仪（Polytec公司的PDV100）进行了比对。实验中所使用的单纵模激光器波长为532 nm，功率为207.7 mW，光折变晶体硅酸铋（BSO）的尺寸为5 mm×5 mm×5 mm，光电探测器的带宽为200 MHz，光敏面直径为500 μm，数据采集卡的带宽为100 MHz，采样速率为250 MS/s。

压电陶瓷PZT上施加如图8(a)所示的正弦电压，其幅值为0.9 V，频率为2 kHz，进而驱动紫铜片做同频率的正弦振动。将参考光与信号光的光强比m调为7.84，参考光与信号光的夹角调为9°，施加在两块BSO晶体上的电压分别为2 500 V和−2 500 V，差动式双波混合干涉仪的测量结果如图8(b)所示，与图5的仿真结果相符，两路输出信号的频率、波形均与施加在压电陶瓷PZT上的正弦电压相同，经过差分处理后，其灵敏度与单路式结构相比提高了一倍。为验证文中压电陶瓷振动测量的有效性，同时采用Polytec公司的激光测振仪（型号：PDV100）进行比对实验，图8(a)为激光测振仪测量结果，与差动式双波混合干涉仪的测量结果相比，二者在波形、频率和相位上具有良好的一致性。

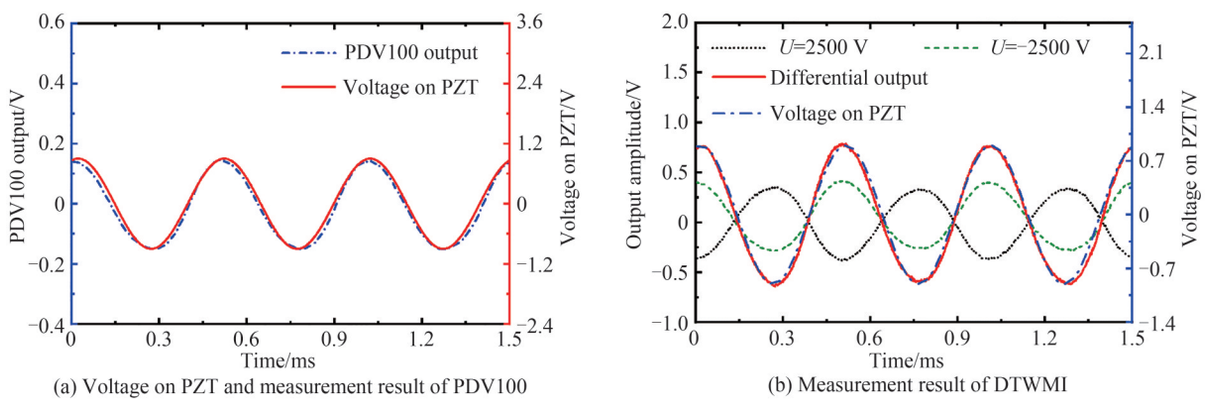

图8 实验中2 kHz正弦振动信号测量结果比对

Fig.8 Comparison of measurement results for sinusoidal vibration of 2 kHz in experiment

对图8(b)中单路和差动式系统的测量结果做频谱分析以研究差动式双波混合干涉仪的噪声抑制能力，分析结果如图9所示，两者的主频均为振动信号频率（2 kHz），与单路的测量结果（信噪比27.78 dB）相比，差动式系统（信噪比30.67 dB）明显抑制了谐波噪声（4 kHz及6 kHz处），且对低频噪声（如交流电网噪声及其谐波）更不敏感。

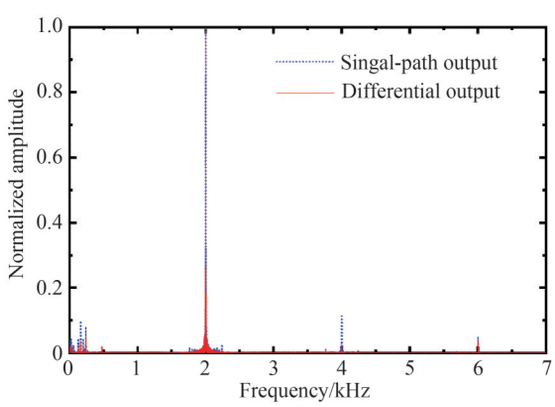

图9 实验中2 kHz正弦振动测量结果频谱分析图

Fig.9 Spectrum analysis of measurement results for sinusoidal vibration with 2 kHz in experiment

为研究系统对高频振动信号的测量能力，在压电陶瓷上施加频率为200 kHz的正弦电压，差动式双波混合干涉仪的测量结果如图10所示，其输出波形无失真，信号主频为200 kHz，且优于PDV100激光测振仪的最高测量频率22 kHz，因此，差动式双波混合干涉仪适用于高频振动的测量，且测量带宽广。

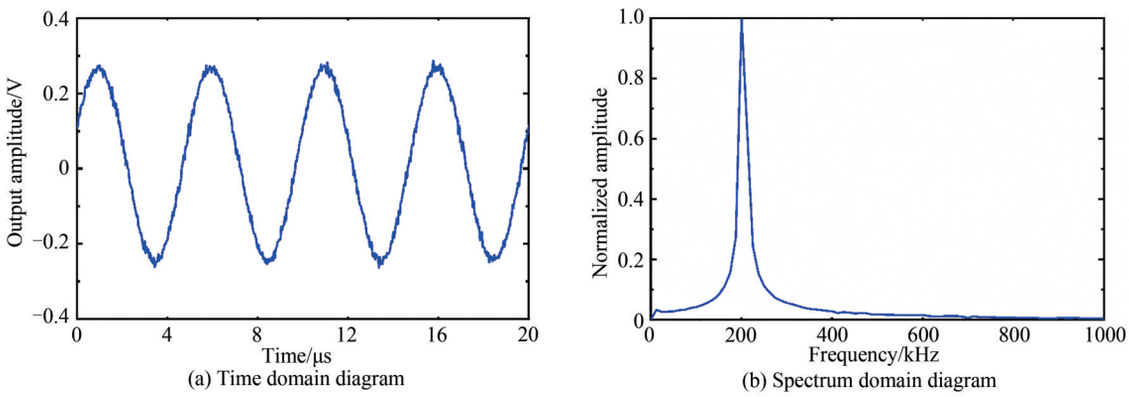

图10　实验中200 kHz正弦振动的测量结果

Fig.10　Measurement result of sinusoidal vibration with 200 kHz in experiment

在压电陶瓷PZT上施加不同幅值的正弦电压，进而驱动紫铜片做不同强度的正弦振动，差动式双波混合干涉仪的输出幅值如图11所示，与图6的仿真结果一致，当被测工件振动幅值小于40 nm时，干涉仪差分输出电压与振动幅值成近似线性关系，利用最小二乘法拟合的非线性误差为2.41%，而当振动幅值进一步增大时，二者成正相关。由图8和图11可得，利用本文所提出的基于差动式双波混合干涉系统可准确获得金属粗糙表面振动的频率、相位及幅值信息。

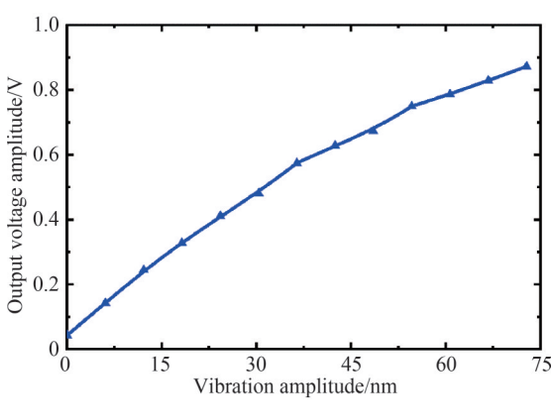

图11　实验中差分输出电压与被测振动幅值的关系

Fig.11　Relationship between differential output voltage and measured vibration amplitude in experiment

为了验证所提系统的稳定性，对系统进行了稳定性测试，在实验中保持施加在压电陶瓷上电压的幅值(0.9 V)与频率(2 kHz)不变，每间隔5 min记录一次系统输出振幅，总共记录20次。每一次测量幅值与幅值均值的相对残余误差如图12所示，差动式双波混合干涉系统的相对误差峰峰值和RMS值分别为4.11%与1.42%，均优于单路式双波混合干涉仪的8.69%与3.07%。因此本文所提出的差动式双波混合干涉系统具有更好的稳定性和可靠性。

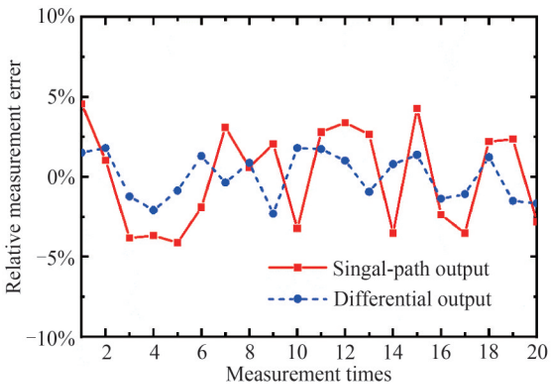

图 12 测量稳定性实验结果

Fig.12 Measurement stability test results

4 结论

为满足金属粗糙表面微小振动的检测需求，本文提出了一种基于差动式双波混合干涉的微小振动检测系统。在两块BSO光折变晶体上施加极性相反的高电压进而引入差动式双光路，并通过光电探测器得到被BSO光折变晶体解调的双路光强信号，对双路信号进行差分处理以获得最终的测量结果，进而抑制单次测量误差与对电压极性不敏感的噪声。对所提出的系统分别进行了仿真分析与实验测量，通过与激光测振仪和单路式系统的对比及重复性实验，表明该系统具有较高的测量准确性及噪声抑制能力，且其带宽明显优于激光干涉仪，其中差动式系统所测结果的信噪比为30.67 dB，非线性误差为2.41%，稳定性的相对误差峰峰值与RMS值分别为4.11%与1.42%。所提出的系统明显优于传统的双波混合干涉仪，可为实现工业环境下高灵敏度、高稳定性和高信噪比的金属粗糙表面微小振动检测提供一种有效可行的手段。

参考文献

[1] YANG Gongxian, LIANG Sen, WANG Guanghe, et al. Vibration analysis of co-cured damping film clamped composite beams[J]. Journal of Vibration and Shock, 2022, 41(9): 90-98.
杨功先, 梁森, 王光和, 等. 共固化阻尼薄膜夹嵌复合材料梁的振动分析[J]. 振动与冲击, 2022, 41(9): 90-98.

[2] YAO Qishui, XIANG Lei, LI Chao, et al. Dynamic characteristic analysis of cylindrical roller bearings[J]. Journal of Vibration Engineering, 2020, 33(4): 734-741.
姚齐水, 向磊, 李超, 等. 新型圆柱滚子轴承动态特性分析[J]. 振动工程学报, 2020, 33(4): 734-741.

[3] PEREIRA J C, ZUBIRI F, GARMENDIA M J, et al. Study of laser metal deposition additive manufacturing, CNC milling, and NDT ultrasonic inspection of IN718 alloy preforms[J]. The International Journal of Advanced Manufacturing Technology, 2022, 120(3): 2385-2406.

[4] YANG K, RONGONG J A, WORDEN K. Damage detection in a laboratory wind turbine blade using techniques of ultrasonic NDT and SHM[J]. Strain, 2018, 54(6): e12290.

[5] LIU Y, YANG S, LIU X. Detection and quantification of damage in metallic structures by laser-generated ultrasonics[J]. Applied Sciences, 2018, 8(5): 824.

[6] LIU Yongqiang, YANG Shixi, GAN Chunbiao. Thickness measurement for thin metal material with the use of laser generated ultrasound[J]. Journal of Vibration and Shock, 2018, 37(12): 147-152.
刘永强, 杨世锡, 甘春标. 一种基于激光超声的薄层金属材料厚度检测方法研究[J]. 振动与冲击, 2018, 37(12): 147-152.

[7] LI Yangyang, WU Sijin, LI Weixian, et al. Simultaneous measurement of displacement and slope with dual-function digital speckle pattern interferometry[J]. Acta Photonica Sinica, 2020, 49(6): 0612002.
李洋洋, 吴思进, 李伟仙, 等. 双功能数字散斑干涉位移及空间梯度同时测量[J]. 光子学报, 2020, 49(6): 0612002.

[8] LI Changyun, WANG Huilin, LIU Kang, et al. Research on intelligent laser triangulation vibration measurement technology[J]. Infrared, 2018, 39(6): 40-44.
李长赟, 王辉林, 柳康, 等. 智能型激光三角法振动测量技术研究[J]. 红外, 2018, 39(6): 40-44.

[9] JANG Y S, LIU H, YANG J, et al. Nanometric precision distance metrology via hybrid spectrally resolved and homodyne interferometry in a single soliton frequency microcomb[J]. Physical Review Letters, 2021, 126(2): 023903.

[10] RZASA J R, CHO K, DAVIS C C. Long-range vibration detection system using heterodyne interferometry[J]. Applied Optics, 2015, 54(20): 6230-6236.

[11] CHANG X, YANG Y, LU J, et al. Vibration amplitude range enhancement method for a heterodyne interferometer[J]. Optics Communications, 2020, 466: 125630.
[12] SHANG Jianhua, REN Lihong, XU Haiqin, et al. Heterodyne laser doppler vibrometer based on double acousto-optic frequency shifters[J]. Acta Photonica Sinica, 2012, 41(10): 1149-1155.
尚建华, 任立红, 徐海芹, 等. 基于双声光移频器的外差式激光多普勒测振计[J]. 光子学报, 2012, 41(10): 1149-1155.
[13] YU Xiangzhi, LI Zhengyong, WANG Zhihao, et al. Effect of temperature and vibration on optical fiber Mach-Zehnder interferometer and dynamic compensation [J]. Acta Photonica Sinica, 2012, 41(9): 1041-1046.
余向志, 李政勇, 王志豪, 等. 温度和振动对光纤马赫-曾德干涉仪的影响与动态补偿研究[J]. 光子学报, 2012, 41(9): 1041-1046.
[14] CHI Feng, ZHU Yu, ZHANG Zhiping, et al. Environment compensation technologies in dual-frequency laser interferometer measurement system[J]. Chinese Journal of Lasers, 2014, 41(4): 190-196.
池峰, 朱煜, 张志平, 等. 双频激光干涉测量中的环境补偿技术[J]. 中国激光, 2014, 41(4): 190-196.
[15] SHCHERBIN K, GVOZDOVSKYY I, SHUMELYUK A, et al. Near-infrared sensitive two-wave mixing adaptive interferometer based on a liquid crystal light valve with a semiconductor substrate[J]. Applied Optics, 2022, 61(22): 6498-6503.
[16] WEI H, KRISHNASWAMY S. Reflective SOA-based fiber Bragg grating ultrasonic sensing system with two wave mixing interferometric demodulation[C]. SPIE, 2017, 10170: 455-463.
[17] KAMSHILIN A A, ROMASHKO R V, KULCHIN Y N. Adaptive interferometry with photorefractive crystals[J]. Journal of Applied Physics, 2009, 105(3): 031101.
[18] HOCHREINER A, REITINGER B, BOUCHAL K D, et al. Quasi-balanced two-wave mixing interferometer for remote ultrasound detection[J]. Journal of Modern Optics, 2013, 60(16): 1327-1331.

Differential Two-wave Mixing Interferometer for Micro-vibration Detection

ZHU Dongxu[1], GONG Yuting[1], LIU Wei[1], KONG Ming[1], WANG Daodang[2]
(1 *College of Metrology and Measurement Engineering, China Jiliang University, Hangzhou* 310018, *China*)
(2 *College of Optical Sciences, University of Arizona, Tucson* 85721, *USA*)

Abstract: With the development of modern manufacturing and testing technology, micro-vibration detection technology for rough metal surface plays an important role in many fields, including material analysis, nondestructive testing, and mechanical system dynamic analysis. The piezoelectric transducer has been widely used in detecting the micro-vibration on rough metal surface, but it is not available to be used on hot or corrosive surface, and hardly to achieve in-line detection for the limited working distance. Several interferometers have been developed for distant detection of micro-vibration, which work well on mirror surface in the laboratory, however, those interferometers can hardly be used to detect micro-vibration of rough metal surface due to the environmental noise and wavefront mismatch.

A micro-vibration detection system based on differential two-wave mixing interference is proposed to meet the requirements of non-contact measurement for micro-vibration on rough metal surface. It provides a simple and elegant solution to these problems arising in the above interferometers, which results from the replacement of a conventional beam splitter with a dynamic holographic grating continuously recorded in a photorefractive crystal. The dynamic holographic grating is modulated by the interference fringe and presents the same distribution, but the change of dynamic holographic grating is available only when the time constant of photorefractive crystal is larger than the change frequency of the interference pattern, which contributes to the fact that the proposed system has the ability of low-frequency noise suppression in non-laboratory environment. The dynamic holographic grating in the photorefractive crystal adapts the reference wavefront to the signal beam, which enables the vibration measurement on rough surface of metal. To reduce the fluctuation of the beam intensity, electric noise, and single measurement error, the proposed system adopts two nonlinear $Bi_{12}SiO_{20}$ (BSO) photorefractive crystals to demodulate the vibration signals in the system. Two BSO photorefractive crystals are applied with high voltage of opposite

polarity to obtain the dual-path signals with opposite polarity, by adopting differential processing to the dual-path signals, the noise insensitive to voltage polarity can be suppressed and the sensitivity to vibration can be improved. Simulation analysis is carried out to verify the feasibility of the proposed detection system, the simulation results show that the dynamic holographic grating is non-shifted or shifted by half of the grating period with respect to the interference fringes when the two BSO photorefractive crystals are applied with high voltage of positive or negative respectively, which contributes to the dual-path output beam intensity with an opposite polarity. By comparing the time domain diagram of vibration signal and output beam intensity in simulation, the capability of the proposed system to measure micro-vibration is affirmed. By calculating the amplitude of the output beam intensity corresponding to vibration signals of different amplitudes, the relationship between them can be achieved, from which an approximate linear relationship between the output beam intensity amplitude and the vibration signals amplitude can be known. To evaluate the noise suppression capability of the proposed system, Gaussian noise and high frequency noise is added to the laser intensity, the simulation result shows the added noise is effectively suppressed by the proposed system. A prototype has been built to further validate the feasibility of the proposed system. The vibration measurement experiment of a copper sheet connected to the piezoelectric transducer is carried out, and the measurement result of the proposed system is compared with the voltage applied to the piezoelectric transducer and the commercial laser vibrometer, the time domain diagram of them has an excellent consistency. Compared with the traditional single-path system, the sensitivity of the proposed system is doubled, the noise is suppressed, and the signal-to-noise ratio is increased from 27.47 dB to 30.83 dB. The relationship between the output voltage amplitude of the proposed system and the measured vibration amplitude can be obtained by applying various voltage amplitude to the piezoelectric transducer, which indicates that the proposed system has an exceptional linearity (the nonlinear error is 2.41% when the vibration amplitude is smaller than 40 nm). The vibration measurement with a frequency of 200 kHz is carried out to evaluate the capability of the proposed system for detecting the high frequency vibration, which is better than the maximum measuring frequency of commercial laser vibrometer (20 kHz). To verify the stability of the system proposed in this paper, the repeatability experiment was conducted, in which the copper sheet was measured 20 times and the measurement interval was 5 min, the relative residual error of each measured amplitude and average amplitude is calculated, the result of experiment shows that the peak to peak value and RMS value of the relative residual error in the proposed system are 4.11% and 1.42% respectively, which is better than the 8.69% and 3.07% in the traditional single-path system. The proposed detection system has high bandwidth and sensitivity with strong noise suppression ability, which provides an effective and feasible method for micro-vibration measurement of rough metal surface in an industrial environment.

Key words: Two-wave mixing interferometer; Differential structure; Micro-vibration detection; Noise suppression; $Bi_{12}SiO_{20}$ crystal

OCIS Codes: 120.3180; 120.4640; 120.7280; 120.1088

Foundation item: Zhejiang Provincial Natural Science Foundation of China (No. LY21E050016), National Natural Science Foundation of China (No. 51775528)